ARTICLE
Journal of Cellular Biochemistry 117:599–611 (2016)

Journal of Cellular Biochemistry

Accelerated Fracture Healing in Transgenic Mice Overexpressing an Anabolic Isoform of Fibroblast Growth Factor 2

Marja M. Hurley,[1]* Douglas J. Adams,[2] Liping Wang,[3] Xi Jiang,[3] Patience Meo Burt,[1] Erxia Du,[1] and Liping Xiao[1]*

[1]*Department of Medicine, University of Connecticut School of Medicine, UCONN Health, Farmington, Connecticut 06030-052*

[2]*Department of Orthopaedic Surgery, University of Connecticut School of Medicine, UCONN Health, Farmington, Connecticut 06030-052*

[3]*Department of Craniofacial Sciences, University of Connecticut School of Dental Medicine, UCONN Health, Farmington, Connecticut 06030-052*

ABSTRACT

The effect of targeted expression of an anabolic isoform of basic fibroblast growth factor (FGF2) in osteoblastic lineage on tibial fracture healing was assessed in mice. Closed fracture of the tibiae was performed in Col3.6–18 kDa*Fgf2*-IRES-GFPsaph mice in which a 3.6 kb fragment of type I collagen promoter (Col3.6) drives the expression of only the 18 kD isoform of FGF2 (18 kDa*Fgf2*/LMW) with green fluorescent protein-sapphire (GFPsaph) as well as Vector mice (Col3.6-IRES-GFPsaph, Vector) that did not harbor the FGF2 transgene. Radiographic, micro-CT, DEXA, and histologic analysis of fracture healing of tibiae harvested at 3, 10 and 20 days showed a smaller fracture callus but accelerated fracture healing in LMWTg compared with Vector mice. At post fracture day 3, FGF receptor 3 and Sox 9 mRNA were significantly increased in LMWTg compared with Vector. Accelerated fracture healing was associated with higher FGF receptor 1, platelet derived growth factors B, C, and D, type X collagen, vascular endothelial cell growth factor, matrix metalloproteinase 9, tartrate resistant acid phosphatase, cathepsin K, runt-related transcription factor-2, Osterix and Osteocalcin and lower Sox9, and type II collagen expression at 10 days post fracture. We postulate that overexpression of LMW FGF2 accelerated the fracture healing process due to its effects on factors that are important in chondrocyte and osteoblast differentiation and vascular invasion. J. Cell. Biochem. 117: 599–611, 2016.

KEY WORDS: LMW Fgf2 ISOFORM MICE; FRACTURE REPAIR; FGFR3; Sox9; PDGF-B; PDGF-C; PDGF-D; VEGF; MMP9; Runx2; OSTERIX; OSTEOCALCIN

Bone repair after fracture or injury is a complex process involving multiple cell types including inflammatory, immune, vascular, and skeletal cells [Einhorn, 1998; Bigham-Sadegh and Oryan, 2014]. It is now well known that many of the same growth factors/cytokines that mediate tissue response to injury are present in skeletal tissue and they mediate normal bone homeostasis, and repair in response to trauma [Bostrom et al., 1995; Einhorn, 1998].

Fibroblast growth factor-2 (FGF2) has been shown to be important in bone formation and maintenance of bone mass [Hurley et al., 2008]. FGF2 is synthesized by osteoblast/stromal cells and stored in the extracellular matrix [Gospodarowicz, 1990]. Knockout of the Fgf2 gene in mice resulted in impaired bone formation that was more evident as the mice aged [Montero et al., 2000]. Our studies show that the exported low molecular weight isoform of FGF2 (LMW) is a critical determinant of bone mass in mice [Xiao et al., 2009]. Recently we published that LMW overexpression in preosteoblast cells promotes bone regeneration in critical size calvarial defects in mice which is partially due to increased osteoblast activity and increased canonical Wnt signaling [Xiao et al., 2014].

Although studies have shown that FGF2 is expressed in the early phase of fracture repair in the granulation tissue at the fracture site [Scully et al., 1990], the role of local application of FGF2 to enhance fracture healing has been controversial [Nakajima et al., 2001; Fei et al., 2013]. Several studies using osteotomy models reported that FGF2 promoted fracture healing by the stimulation of callus

Grant sponsor: National Institute of Aging; Grant number: R01AG021189.

*Correspondence to: Marja M. Hurley and Liping Xiao, Department of Medicine, University of Connecticut School of Medicine, UCONN Health, Farmington, CT 06030-052.
E-mail: hurley@uchc.edu (M.H.H.) and xiao@uchc.edu (L.X.)

Manuscript Received: 3 August 2015; Manuscript Accepted: 4 August 2015
Accepted manuscript online in Wiley Online Library (wileyonlinelibrary.com): 7 August 2015
DOI 10.1002/jcb.25308 • © 2015 Wiley Periodicals, Inc.

remodeling in canine tibial fracture [Nakamura et al., 1998] and increased periosteal ossification and bone callus formation in a rat fibula fracture model [Kawaguchi et al., 1994] and rabbit fibula [Radomsky et al., 1998] whereas injection of FGF2 into rabbit tibial fracture had no effect on healing [Bland et al., 1995]. A local application of the rhFGF-2 hydrogel accelerated healing of tibial shaft fractures with a safety profile in humans [Kawaguchi et al., 2010]. β-tricalcium phosphate granules, hyaluronate, and FGF2 promote repair of unstable intertrochanteric fractures in patients [Tanaka et al., 2012]. FGF2 administered in a biodegradable gelatin hydrogel accelerated fracture healing in an osteotomy model in non-human primates [Radomsky et al., 1999; Kawaguchi et al., 2001]. Komaki et al. [2006] reported that FGF2 complexed with calcium and collagen repaired segmental defects in rabbit tibiae. In contrast closed fractures in rats showed that exogenous FGF2 enlarged the cartilaginous callus but did not induce rapid healing of femoral fractures [Nakajima et al., 2001]. The authors Nakajima et al. [2001] postulated that these different/varied results might reflect different effects of FGF2 in osteotomy versus closed fracture models. It is also possible that the dose and frequency of administration of FGF2 could modulate its effect on fracture healing. In view of these conflicting reports, we examined the role of targeted over-expression of the anabolic LMWFGF2 in the osteoblastic lineage on fracture repair using a closed fracture model of the tibiae of LMW transgenic mice (LMWTg) as well as control (Vector) mice.

Surprisingly, there is limited data on FGF2 modulation of gene expression during fracture healing [Nakajima et al., 2001], we also assessed quantitatively the temporal effects of LMWTg on genes important in the different stages of fracture repair. These results demonstrated that LMWFGF2 accelerated fracture healing via enhanced expression of known as well as novel genes.

MATERIALS AND METHODS

ANIMALS

As previously described in detail by Xiao et al. [2009] we generated mice expressing 18 kD isoform of hFGF2 in a bone-specific manner using a construct, abbreviated Col3.6–18 kDFgf2 isoform-IRES-GFPsaph. Col3.6–18 kDFgf2 isoform-IRES-GFPsaph was built by replacing a CAT fragment in previously made Col3.6-CAT-IRES-GFPsaph [Kalajzic et al., 2002] with a human LMW cDNA between Afe I and Sca I sites. This expression construct is capable of concurrently overexpressing the LMW [Xiao et al., 2003] and GFPsaph from a single bicistronic mRNA. The construct also harbors a neomycin selection gene. Generation of the Fgf2 cDNAs was previously described by Florkiewicz and Sommer [1989]. As control a Col3.6-IRES/GFPsaph (Vector) construct was also generated and purified according to standard techniques. Microinjections into the pronucleus of fertilized oocytes were performed at the Gene Targeting & Transgenic Facility at the University of Connecticut Health Center. Founder mice of the F2 (FVBN) strain were mated with wild-type mice to establish individual transgenic lines. Homozygote mice were generated by mating heterozygote male with heterozygote female. Initial characterization of the bone phenotype of the LMWTg mice was previously reported by Xiao et al. [2009].

FRACTURE MODEL

Bone fractures were generated as previously described by Bonnarens and Einhorn [1984] and modified for use in mice by Hiltunen et al. [1993]. Eight to 10 week old female mice were utilized. All procedures for producing closed tibial fractures were approved by the University Animal Care Committee. Anesthesia was induced and maintained using inhalant isoflurane (2.0–2.5% delivered in oxygen, 200 ml/min). Analgesia was administered prior to fracture via subcutaneous injection of 0.08 mg/kg Buprenorphine, with further administration of analgesia as indicated by animal behavior. Closed fractures of the right tibia were generated using the common method of drop-weight blunt guillotine, producing uniform transverse fractures at mid-diaphysis approximately 3 mm proximal to the distal fibular junction. Prior to fracture, a solid 27-gage (0.01" diameter) 316LVM stainless steel rod (Small Parts, Inc.) was inserted antegrade into the medullary canal. An initial intramedullary channel was established through the tibial plateau and proximal tibia using a 26-gage needle. After placing the intramedullary fixation rod, the limb was placed in the guillotine device, contact supports tightened to the tibia, and a single drop of the weight applied to achieve a transverse tibia fracture without fracturing fibular. Digital radiographs were acquired to verify fracture location and severity. Animals ambulated with partial weight-bearing within 10 min of removing anesthesia. Twenty-four hour prior to sacrifice, mice were injected with xylenol orange (0.09 mg/g body weight) to assess newly formed deposited mineral content. Mice were euthanized by CO_2 narcosis and cervical dislocation at post fracture day 3 (PFD3), post fracture day 10 (PFD10) and post fracture day 20 (PFD20). Intra-medullary pins were removed after the mice were sacrificed and radiographs were obtained before removal of the pins.

RADIOLOGY

Bone radiographs were obtained with a SYSTEM MX 20 from Faxitron X-ray Corporation. Imaging of the architecture of the fracture callus was performed using X-ray micro-CT (μCT-40, Scanco Medical, Bassersdorf). The tibiae then were prepared for frozen sectioning, or decalcified and paraffin embedded for histology and immunohistochemical analysis.

HISTOLOGY

For histological analysis, the tibiae were immediately fixed in 4% PFA at 4°C. After processing samples were embedded in Shandon Cryomatrix (Thermo Electron Corporation, Pittsburgh, PA) and completely frozen. The other tibiae were decalcified in 20% EDTA in PBS for 2 days, and paraffin blocks were prepared by standard procedures. Paraffin or frozen samples were cut into 5 μm sections. Frozen sections were stained with Alcian Blue to identify cartilage matrices and with Alizarin Red to identify bone. For the histomorphometic analysis, perimeters of cartilaginous and bony callus were outlined. The outlined regions of the cartilage callus area, bony callus area and total callus area were measured using Osteomeasure bone morphometry analysis software. Frozen sections were scanned to detect GFP and xylenol orange labeling of bone cells. GFP expression in cells was visualized using an Olympus IX50 inverted system

microscope equipped with an IX-FLA inverted reflected light fluorescence (Olympus America, Inc., Melville, NY). A specific excitation wavelength was obtained using filters for GFPsaph (exciter, D395/40; dichroic, 425DCLP; emitter, D510/40 m) and recorded with a SPOT-camera (Diagnostic Instrument, Inc., Sterling Heights, MI). Fluorescent images were taken with equal exposure times applied to bones derived from Vector and LMWTg mice.

Paraffin embedded sections were used for immnuno-histochemistry of type XI collagen; MMP9, cathepsin K (CTSK), VEGF, FGF2, and RUNX2 (Santa Cruz Biotechnology Corp, Santa Cruz, CA); Osterix (ABCAM Diagnostics, Cambridge, MA), SOX 9 (ABCAM), PDGFB, PDGFC, PDGFD (Bioss Inc. Woburn, MA). Histochemical detection of tartrate resistant acid phosphatase (TRAP) (Kamiya Biomedical Company, Seattle, WA) was conducted as described previously by Amizuka et al. [2004]; [Li et al., 2006]. Sections from three mice per group were used for staining.

RNA ISOLATION AND REAL-TIME PCR

Total RNA was extracted from the fracture calluses using Trizol reagent (Invitrogen Life Technologies, Carlsbad, CA). For real-time quantitative RT-PCR (qRT-PCR) analysis, RNA was reverse-transcribed by the Super-Script^{TM} First-Strand Synthesis System. qPCR was carried out using the QuantiTect^{TM} SYBR Green PCR kit (Qiagen) on a MyiQ^{TM} instrument (BIO-RAD Laboratories Inc. Hercules, CA). β-Actin was used as an internal reference for each sample. mRNA was normalized to the β-Actin mRNA level and expressed as the fold-change relative to the first sample for each experimental group. Relative mRNA expression was calculated using a formula reported previously by Pfaffl [2001]. The primers for the genes of interest are listed in Table I.

STATISTICAL ANALYSIS

Experimental values are reported as mean ± standard error (SEM). ANOVA followed by Least Significant Difference (LSD) for Post Hoc Multiple Comparisons were used. SPSS software was used for statistical analysis, and the results were considered significantly different at $P < 0.05$.

RESULTS

RADIOGRAPHIC AND MICROCT ANALYSIS OF FRACTURE HEALING IN VECTOR AND LMWTg MICE

To determine the effects of expression of LMW targeted to pre-osteoblastic cells on the process of fracture healing, we generated closed stabilized tibial fractures in Vector and LMWTg mice and examined the healing process at different stages. As shown by plain radiographs (Fig. 1A), there was no evidence of callus formation at PFD3 in either genotype. At PFD10 there was radiographic (Fig. 1A) evidence of a bony bridge in LMWTg compared with Vector control mice. At PFD10 and PFD20 radiographic (Fig. 1A) and Micro-CT PFD20 (Fig. 1B) showed that the fracture calluses of tibiae from Vector mice were much larger than that observed in tibiae from LMWTg mice.

HISTOLOGIC ANALYSIS OF TIBIAL FRACTURE HEALING IN VECTOR AND LMWTg MICE

In order to qualitatively and quantitatively compare the total callus area and the calcified area, frozen sections of the fracture callus were stained with Alcian Blue to detect cartilage and Alizarin Red for mineral. As shown in Figure 2A, a larger area of Alcian Blue staining was observed in Vector than in the LMWTg at PFD10. There was evidence of on going remodeling of the callus in the Vector at PFD20; in contrast, there appeared to be almost complete remodeling of the fracture in LMWTg mice. Figure 2B shows greater expression of GFP in the periosteum and at the healing fracture site and in osteocytes of the LMWTg mice at PFD20 (arrows). Examination of the growth plate revealed no increased expression of GFP in columnar chondrocytes or hypertrophic chondrocytes in either the Vector or LMWTg mice (data not shown). At PFD20, there was increased xylenol orange (XO) labeling reflecting new mineral deposition in the Vector compared with the LMWTg that appeared to have completed the remodeling phase. This indicates that at PFD20 the callus remodeling was almost complete in LMWTg, while in Vector mice large mineralizing bone callus was still undergoing remodeling. Figure 2C–E show the results of quantitative analysis of the turnover of cartilage to bone in the fracture callus expressed as total

TABLE I. Primers Used in qRT-PCR

β-*Actin*	5′-ATGGCTGGGGTGTTGAAGGT-3′	5′-ATCTGGCACCACACCTTCTACAA-3′
Col2	5′-CAGGATGCCCGAAAATTAGGG-3′	5′-ACCACGATCACCTCTGGGT-3′
Col10	5′-GGGACCCCAAGGACCTAAAG-3′	5′-GCCCAACTAGACCTATCTCACCT-3′
Ctsk	5′-GAAGAAGACTCACCAGAAGCAG-3′	5′-TCCAGGTTATGGGCAGAGATT-3′
Fgf2	5′-GTCACGGAAATACTCCAGTTGGT-3′	5′-CCCGTTTTGGATCCGAGTTT-3′
Fgf18	5′-AAGGAGTGCGTGTTCATTGAG-3′	5′-AGCCCACATACCAACCAGAGT-3′
Fgfr1	5′-GAC TGC TGG AGT TAATACCA-3′	5′-CTG GTC TCT CTT CCA GGG CT-3′
Fgfr2	5′-CTGTGGGCTGAAGGCATT-3′	5′-CCCTGGTCCTCTTCCATATCT-3′
Fgfr3	5′-GTTCTCTCTTTGTAGACTGC-3′	5′-AGTACCTGGCAGCACCA-3′
Mmp9	5′-GCGTCGTGATCCCCACTTAC-3′	5′-CAGGCCGAATAGGAGCGTC-3′
Mmp13	5′-CTTTGGCTTAGAGGTGACTGG-3′	5′-AGGCACTCCACATCTTGGTTT-3′
Ocn	5′-GAGGGCAATAAGGTAGTGAACAGA-3′	5′-AAGCCATACTGGTTTGATAGCTCG-3′
Osterix	5′-ACTGGCTAGGTGGTGGTCAG-3′	5′-GGTAGGGAGCTGGGTTAAGG-3′
Pdgf a	5′-GAGGAAGCCGAGATACCCC-3′	5′-TGCTGTGGATCTGACTTCGAG-3′
Pdgf b	5′-CATCCGCTCCTTTGATGATCTT-3′	5′-GTGCTCGGGTCATGTTCAAGT-3′
Pdgf c	5′-GCCAAAGAACGGGGACTCG-3′	5′-AGTGACAACTCTCTCATGCCG-3′
Pdgf d	5′-ATGCAACGGCTCGTTTTAGTC-3′	5′-CGGAGTCGCAAAAGTGTCC-3′
Pdgfra	5′-ATGAGAGTGAGATCGAAGGCA-3′	5′-CGGCAAGGTATGATGGCAGAG-3′
Pdgfrb	5′-TTCCAGGAGTGATACCAGCTT-3′	5′-AGGGGGCGTGATGACTAGG-3′
Runx2	5′-ACAAACAACCACAGAACCACAAAGT-3′	5′-GTCTCGGTGGCTGGTAGTGA-3′
Sox9	5′-AGTACCCGCATCTGCACAAC-3′	5′-ACGAAGGGTCTCTTCTCGCT-3′
Trap	5′-CACTCCCACCCTGAGATTTGT-3′	5′-CATCGTCTGCACGGTTCTG-3′
Vegf	5′-GCACATAGAGAGAATGAGCTTCC-3′	5′-CTCCGCTCTGAACAAGGCT-3′

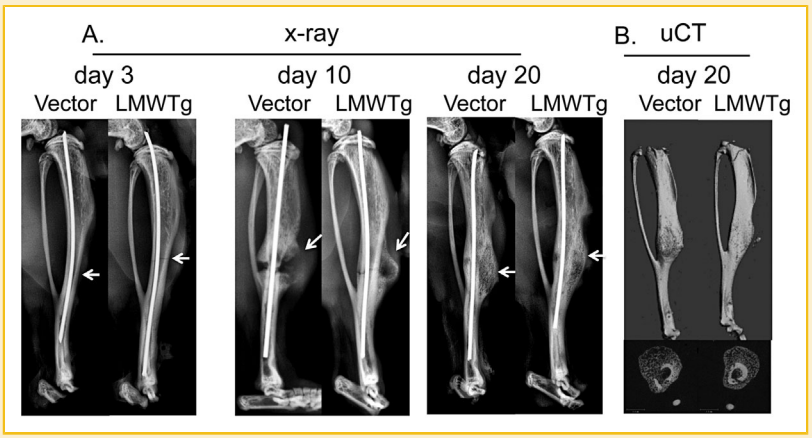

Fig. 1. Radiologic analysis of tibial fracture healing in Vector and LMWTg mice. (A) Plain radiographs of representative fractured tibiae at post fracture day 3–20 in Vector and LMWTg mice. Arrows show the fracture. (B) Micro-CT images at post fracture day 20. Lower panel shows cross sectional micro-CT images of changes in the calcified area of the callus at the fracture site in Vector and LMWTg mice.

callus area and the ratio of cartilage area or bony area to total area. As shown in Figure 2C there was no callus formation at PFD3. However, at PFD10 total callus area was significantly increased by 34% in the tibiae from Vector mice compared with LMWTg ($P < 0.05$). At PFD20 although the callus was smaller than in PFD10, total callus area was still 21% significantly increased in the tibiae from Vector mice compared with LMWTg ($P < 0.05$). As shown in Figure 2D,E at PFD10 although cartilage area/total callus area was increased in both genotypes, there was a greater increase in Vector (52%, $P < 0.05$). In contrast bony area/total callus area was higher in LMWTg compared with Vector mice

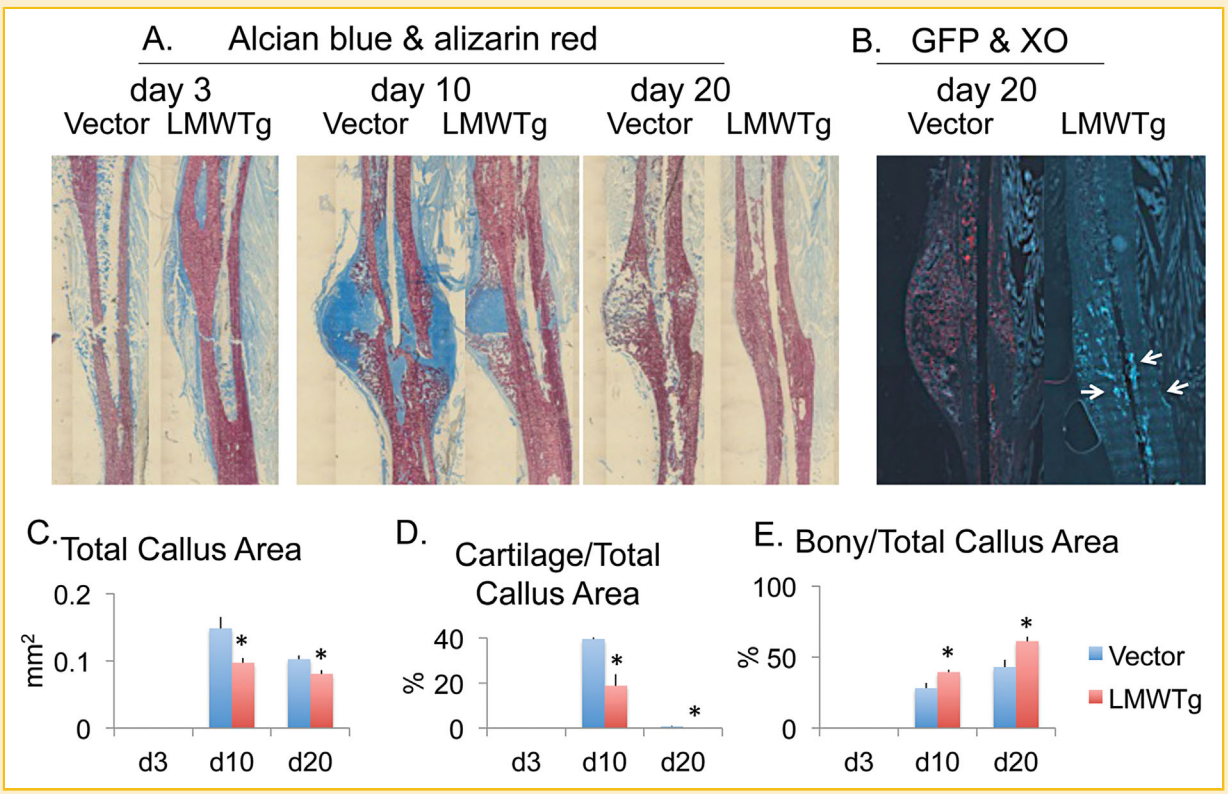

Fig. 2. Histologic analysis of tibial fracture healing in Vector and LMWTg mice. (A) Time course examination of Alcian Blue staining of cartilage and Alizarin Red staining for mineral of frozen sections of the fractured tibiae of Vector and LMWTg mice. (B) Frozen section demonstrating GFPsaph (arrows) and xylenol orange labeling of the fracture callus at 20 days in Vector and LMWTg mice. (C) Total callus area; (D) Ratio of cartilage callus area/total callus area and (E) Ratio of bony callus area/total callus area measured by Osteomeasure. n = 3. Data are the mean ± SEM. *Compared with corresponding Vector $P < 0.05$.

(42%, $P < 0.05$). At PFD20, the cartilage was mostly replaced by bone in both Vector and LMWTg mice. However, the remodeling process resulted in the woven bone being replaced with compact bone in LMWTg mice (Figure 2B,D, and E).

FGF2 AND FGF RECEPTOR EXPRESSION IN TIBIAL FRACTURE HEALING OF VECTOR AND LMWTg MICE

To examine the mechanisms involved in the accelerated fracture healing in LMWTg mice, gene analysis by qPCR and immunohistochemical analysis of the protein products of genes important in fracture healing was performed on fracture calluses harvested at PFD3, PFD10, and PFD20. As shown in Figure 3A Fgf2 mRNA was overexpressed in the fracture callus of LMWTg mice compared with Vector mice at all time points. Fgf2 mRNA expression was similar in Vector at PFD3, PFD10, and PFD20. Comparison of PFD10 callus in tibia from the Vector and LMWTg (Fig. 3B), showed increased FGF2 labeling in osteoblasts on the surface of newly formed woven bone and in osteocytes embedded in woven bone from LMWTg mice.

Fibroblast growth factor 18 (Fgf18) mRNA was increased during fracture healing [Schmid et al., 2009], however, there are no reports of FGF2 regulating FGF18 expression, we therefore examined its temporal and level of expression. Fgf18 mRNA expression was greater in Vector at all time points compared with LMWTg (Supplementary Table S1). Thus accelerated fracture repair in LMWTg is not due to increased FGF18.

We assessed whether there was differential FGF receptor gene expression in the fracture callus of Vector and LMWTg mice. As shown in Figure 3C, compared to corresponding Vector, Fgfr3 mRNA expression was significantly higher at PFD3 in LMWTg. At PFD10, Fgfr3 mRNA was similarly increased in both Vector and LMWTg. However Fgfr3 mRNA was significantly decreased at PFD20 compared with PFD10 in LMWTg. As shown in Figure 3D, compared to corresponding Vector, Fgfr1 mRNA expression was significantly decreased at PFD3, but higher at PFD10 in LMWTg mice. Compared to corresponding PFD3, FGFR1 mRNA expression was increased at PFD10 in both Vector and LMWTg. There was a further increase at

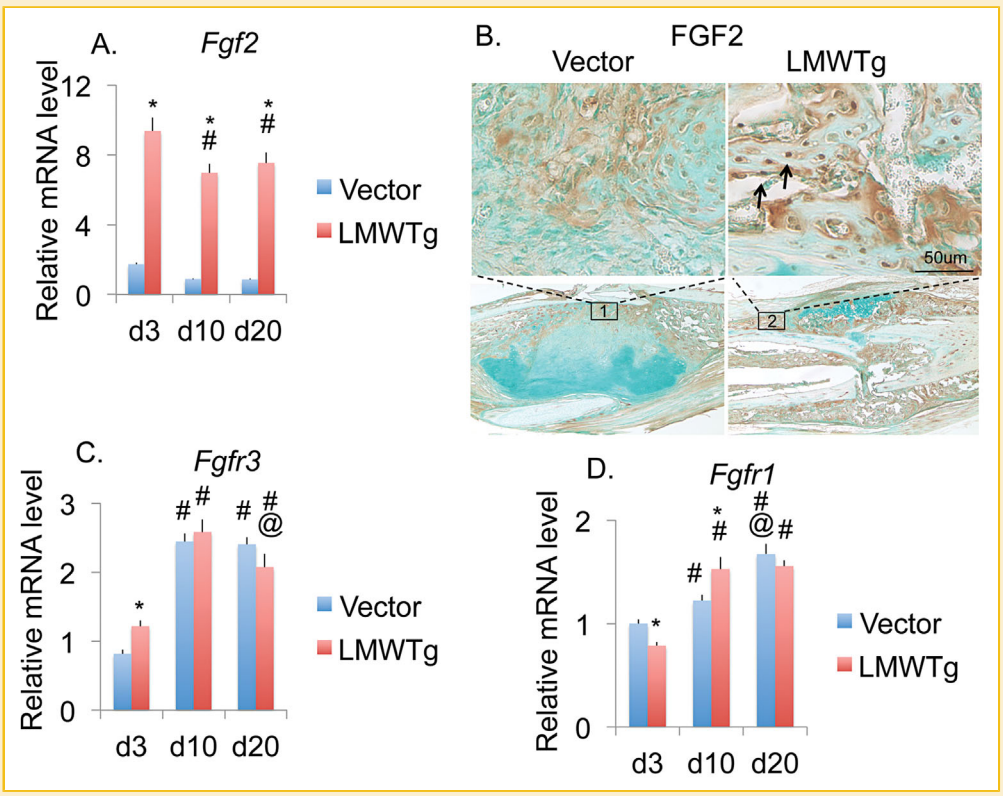

Fig. 3. Fgf2 mRNA and protein, Fgfr3 and Fgfr1 mRNA in tibial fracture healing in Vector and LMWTg mice. (A) qPCR analysis of Fgf2 mRNA expression in the fracture callus of Vector and LMWTg mice at post fracture day (PFD) 3, 10, and 20. Fgf2 mRNA was overexpressed in LMWTg mice compared with Vector mice at all time points. Fgf2 mRNA expression was not significantly altered in Vector among PFD3, 10, and 20 groups. However, Fgf2 mRNA expression was decreased in 10 and PFD20 compared with PFD3 in LMWTg mice. n = 6–11. (B) Immunohistochemistry for FGF2 protein in the fracture callus of Vector and LMWTg mice at PFD10. Note the overexpression of FGF2 (arrows) in osteoblasts on the surface of newly formed woven bone and in osteocytes embedded in woven bone from LMWTg mice. (C) qPCR analysis of Fgfr3 mRNA expression in the fracture callus of Vector and LMWTg mice at 3,10, and PFD20. Compared to corresponding Vector, Fgfr3 mRNA expression was higher at PFD3 in LMWTg mice. Compared to corresponding PFD3, Fgfr3 mRNA expression was increased in both Vector and LMWTg. There was a decrease at PFD20 compared with PFD10 in LMWTg. n = 7–11. (D) Fgfr1 mRNA expression in the fracture callus of Vector and LMWTg mice at 3,10, and PFD20. Compared to corresponding Vector, Fgfr1 mRNA expression was lower at PFD3, but higher at PFD10 in LMWTg mice. Compared to corresponding PFD3, Fgfr1 mRNA expression was increased in both Vector and LMWTg. There was a further increase at PFD20 in Vector compared with PFD10. n = 6–11. Data are the mean ± SEM. *Compared with corresponding Vector $P < 0.05$; #Compared with corresponding PFD3 $P < 005$; @Compared with corresponding PFD10 $P < 0.05$. For immunohistochemistry staining, all insets are 20× magnification of each figure at 4× magnification.

PFD20 in Vector compared with PFD10. The time course of Fgfr2 mRNA analysis revealed a significant reduction in LMWTg at PFD3 compared with Vector, however, at PFD10 and PFD20 similar increased levels was observed in both genotypes (Supplementary Table S1).

SOX9 AND Col2 mRNA AND PROTEIN EXPRESSION IN TIBIAL FRACTURE OF VECTOR AND LMWTg MICE

The mRNA and protein products of the Sox9 gene as well as type II collagen (Col2a1), chondrocyte differentiation markers, were determined. Sox9 is a transcription factor that is involved in up-regulation of the Col2a1 gene [Sakano et al., 2000]. As shown in Figure 4A, compared to corresponding Vector, Sox9 mRNA expression was significantly higher at PFD3, but lower at PFD10 in LMWTg mice. In LMWTg mice, Sox9 mRNA expression was significantly decreased at PFD20 compared with PFD3 and PFD10. In Vector mice, Sox9 mRNA expression was increased at PFD10 then decreased at PFD20. Immunohistochemistry for SOX9 protein is shown in the fracture callus of Vector and LMWTg mice at PFD10 (Fig. 4B). There was a marked increase in SOX9 protein in chondrocytes and osteocytes of Vector mice.

Figure 4C shows analysis of Col2a1 mRNA expression in the fracture callus of Vector and LMWTg mice. In both Vector and LMWTg mice, compared with PFD3, Col2a1 expression was significantly increased at PFD10. However at PFD10, Col2a1 mRNA was significantly lower in LMWTg mice compared with Vector consistent with enhanced chondrocyte differentiation in LMWTg. Immunohistochemistry of the fracture callus at PFD10 (Fig. 4D) showed higher expression of COL2 in chondrocytes in Vector compared with LMWTg mice.

PLATELET DERIVED GROWTH FACTOR EXPRESSION IN TIBIAL FRACTURE IN VECTOR AND LMWTg MICE

Platelet derived growth factor expression during fracture repair has also been reported in many studies [Hadjiargyrou and O'Keefe, 2014] and PDGF potentiates FGF2-stimulated vascular endothelial cell growth factor (VEGF) release in osteoblast [Tokuda et al., 2008]. Since there are four PDGF genes, the mRNA expression of all four genes; platelet derived growth factor A, (Pdgfa); platelet derived growth factor B (Pdgfb), platelet derived growth factor C (Pdgfc), and platelet derived

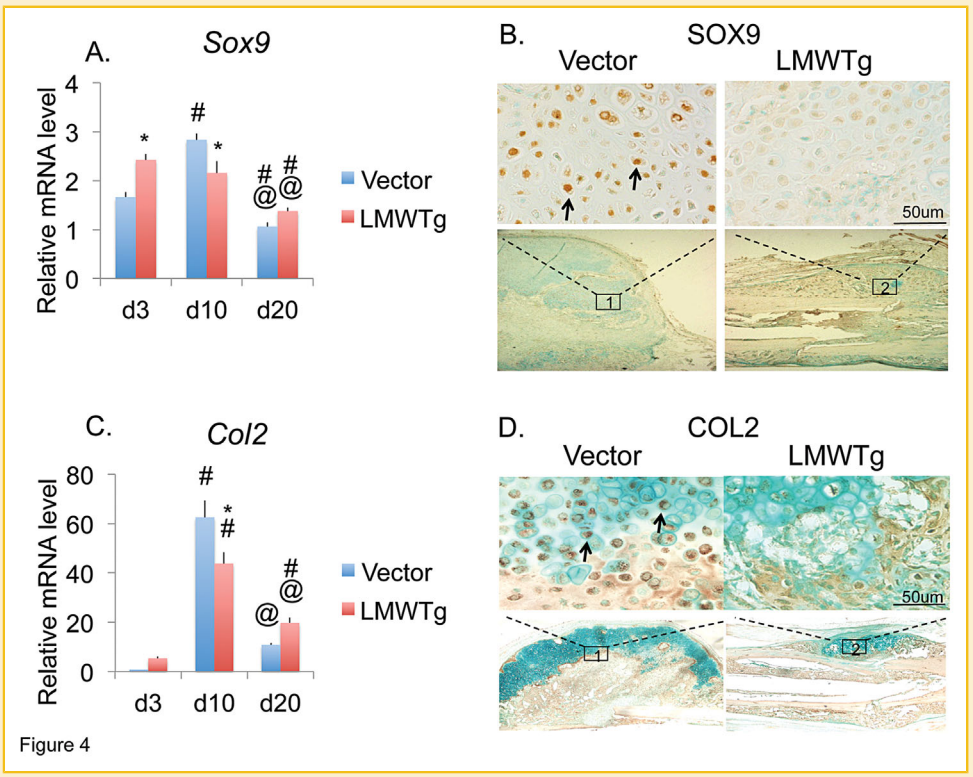

Fig. 4. Sox9 and Col2 mRNA and protein expression in tibial fracture healing in Vector and LMWTg mice. (A) Sox9 mRNA in the fracture callus of Vector and LMWTg mice at post fracture day (PFD) 3,10, and 20. Compared to corresponding Vector, Sox9 mRNA was increased at PFD3, but decreased at PFD10 in LMWTg mice. In Vector mice, Sox9 mRNA was increased at PFD10 but decreased at PFD20. In LMWTg mice, Sox9 mRNA expression was low at PFD20 compared with 3 and PFD10. n = 7–10. (B) Immunohistochemistry for SOX9 protein in the fracture callus of Vector and LMWTg mice at PFD10. Note increased SOX9 (arrows) in chondrocytes and osteocytes of Vector mice. (C) Col2 mRNA expression in the fracture callus of Vector and LMWTg mice at 3, 10, and PFD20. At PFD10, Col2 mRNA was decreased in LMWTg mice compared with Vector. In both Vector and LMWTg mice, Col2 increased at PFD10, then decreased at PFD20. n = 7–11. (D) Immunohistochemistry for COL2 protein in the fracture callus of Vector and LMWTg mice at PFD10. Note the higher expression of COL2 (arrows) in chondrocytes in Vector mice. Data are the mean ± SEM. *Compared with corresponding Vector $P < 0.05$; #Compared with corresponding d3 $P < 005$; @Compared with corresponding d10 $P < 0.05$. For immunohistochemistry staining, all insets are 20× magnification of each figure at 4× magnification.

growth factor D (Pdgfd) were assessed in the fracture callus of Vector and LMWTg mice at each time point. The mRNA expression levels of Pdgfa were similar between Vector and LMWTg at each time point (Supplementary Table S1). As shown in Figure 5A, Pdgfb mRNA expression was similar between Vector and LMWTg at PFD3. In Vector mice, Pdgfb mRNA expression was significantly increased at PFD10 and further increased at PFD20 compared with PFD3. Compared with corresponding Vector, Pdgfb mRNA expression was significantly higher at PFD10 in LMWTg mice and there was no further increase at PFD20. Higher expression of Pdgfb at PFD10 was confirmed at protein level by immunohistochemistry staining (Fig. 5B). As shown in Figure 5C, Pdgfc mRNA expression was similar between Vector and LMWTg at PFD3. In Vector mice, Pdgfc mRNA expression was significantly increased at PFD10 and further increased at PFD20 compared with PFD10. Compared with corresponding Vector, Pdgfc mRNA expression was significantly higher at PFD10 in LMWTg mice but was significantly decreased compared with corresponding Vector at PFD20. Figure 5D shows the higher PDGFC protein expression in LMWTg mice at PFD10 compared with Vector. Pdgfd mRNA is shown in Figure 5E and expression level was similar between Vector and LMWTg at PFD3. In Vector mice, Pdgfd mRNA expression was significantly increased at PFD10 and further significantly increased at PFD20 compared with PFD3 and PFD10. Compared with corresponding Vector, Pdgfd mRNA expression was significantly higher at PFD10 in LMWTg mice but was similar compared with corresponding Vector at PFD20. As shown in Figure 5F higher PDGFD protein expression was observed in LMWTg mice at PFD10 compared with Vector.

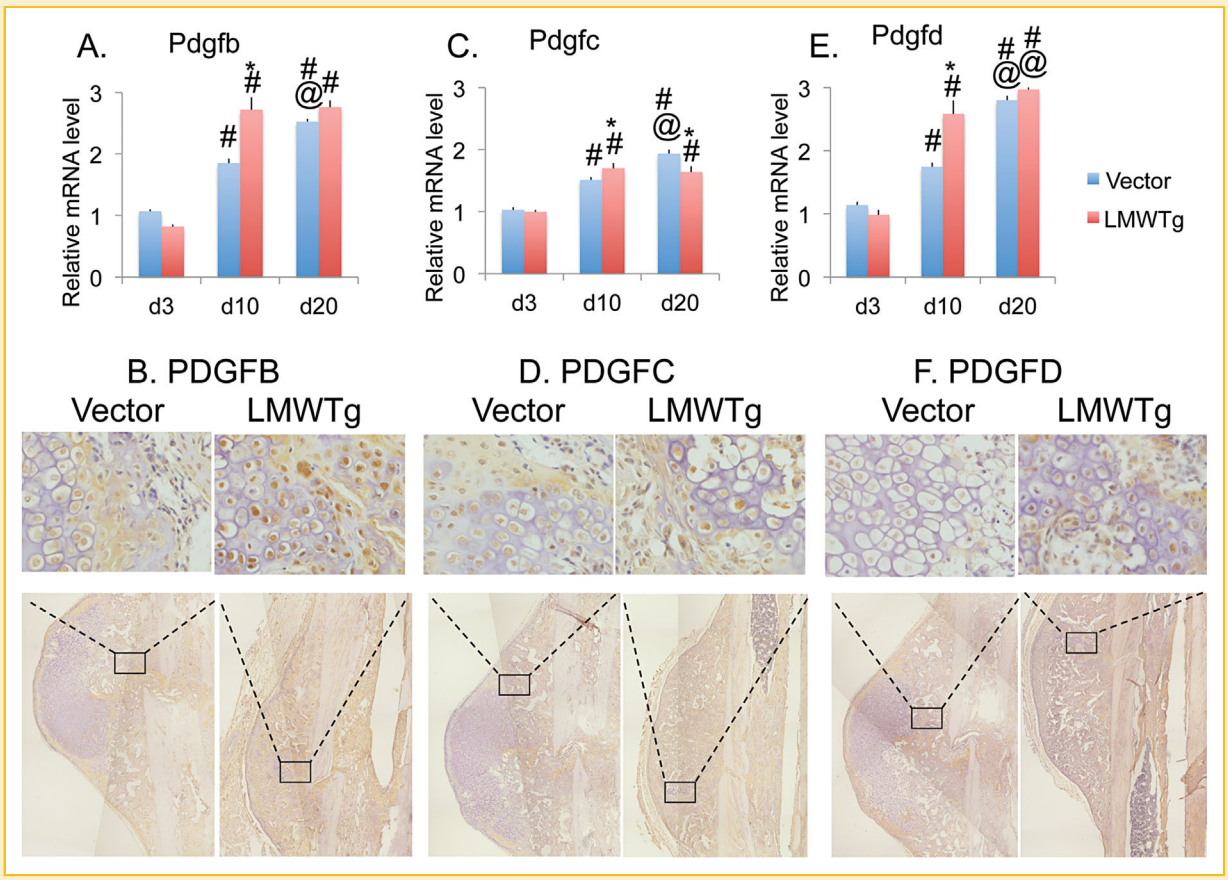

Fig. 5. Pdgfb, Pdgfc, Pdgfd mRNA, and protein expression in tibial fracture healing in Vector and LMWTg mice. (A) Pdgfb mRNA expression in the fracture callus of Vector and LMWTg mice at post fracture day (PFD) 3,10, and 20. Compared with corresponding Vector, Pdgfb mRNA was higher at PFD10 in LMWTg mice and remained elevated at PFD20. In Vector mice, Pdgfb expression was increased at PFD10 and further increased at PFD20. At PFD10 Pdgfb mRNA expression was higher in LMWTg mice compared with Vector mice. n = 7–11. (B) Immunohistochemistry for PDGFB protein in the fracture callus of Vector and LMWTg mice at PFD10. Note higher PDGFB expression in LMWTg mice. (C) Pdgfc mRNA expression in the fracture callus of Vector and LMWTg mice at 3,10, and PFD20. Compared with corresponding Vector, Pdgfc mRNA was higher at PFD10 in LMWTg mice and remained elevated at PFD20. In Vector mice, Pdgfc expression was increased at PFD10 and further increased at PFD20. n = 7–11. (D) Immunohistochemistry for PDGFC protein in the fracture callus of Vector and LMWTg mice at PFD10. Note higher PDGFC expression in LMWTg mice. (E) Pdgfc mRNA expression in the fracture callus of Vector and LMWTg mice at 3,10, and PFD20. Compared with corresponding Vector, Pdgfc mRNA was higher at PFD10 in LMWTg mice and remained elevated at PFD20. In both Vector and LMWTg mice, Pdgfc expression was increased at PFD10 and further increased at PFD20. n = 7–11. (F) Immunohistochemistry for PDGFD protein in the fracture callus of Vector and LMWTg mice at PFD10. Note higher PDGFD expression in LMWTg mice. Data are the mean ± SEM. *Compared with corresponding Vector $P < 0.05$; #Compared with corresponding PFD3 $P < 005$; @Compared with corresponding PFD10 $P < 0.05$. For immunohistochemistry staining, all insets are 20× magnification of each figure at 5× magnification scanning.

TYPE X COLLAGEN, VASCULAR ENDOTHELIAL CELL GROWTH FACTOR AND MATRIX METALLOPROTEINASE-9 EXPRESSION IN TIBIAL FRACTURE HEALING IN VECTOR AND LMWTg MICE

As shown in Figure 6A at PFD10 type X collagen (Col10) mRNA, a marker for hypertrophic chondrocytes was significantly higher in LMWTg compared with Vector.

The expression of other factors important in callus remodeling was also determined. As shown in Figure 6B compared with PFD3, Vegf mRNA was increased at PFD10 and PFD20 in both Vector and LMWTg mice. However, there was a further significant increase at PFD20 in LMWTg compared with PFD10. By immunohistochemistry at PFD10 VEGF protein was robustly expressed by prehypertrophic chondrocytes, hypertrophic chondrocytes, and vascular cells in the bone marrow of both Vector and LMWTg, but VEGF expression was stronger in fracture callus of LMWTg mice (Supplementary Figure S1A) particularly in the areas where bone was replacing the cartilage. On PFD20, VEGF expression remained higher in LMWTg mice compared with Vector (Supplementary Figure S1B).

Matrix metalloproteinase 9 (MMP9) and matrix metalloproteinase 13 (MMP13) are important in fracture repair [Uusitalo et al., 2000; Kosaki et al., 2007]. As shown in Figure 6C compared to corresponding Vector, Mmp9 mRNA expression was increased at PFD10 but was decreased at PFD20 in LMWTg mice. In Vector mice, compared to PFD3, Mmp9 mRNA expression was significantly increased at both PFD10 and PFD20. Immunohistochemistry for MMP9 protein in the fracture callus of Vector and LMWTg mice at PFD10 is shown in Figure 6D. Marked increased in MMP9 expression was observed in hypertrophic chondrocytes of LMWTg mice.

Since MMP13 is involved in breakdown of matrix especially cleavage of type II as well as type I collagen during fracture healing [Yamagiwa et al., 1999], changes in MMP13 mRNA was examined. At PFD3 Mmp13 mRNA expression was similar in Vector and LMWTg and there was a similar progressive increase in Mmp13 mRNA at PFD10 and at PFD20 in both genotypes (Supplementary Table S1).

TRAP AND CATHEPSIN K mRNA AND PROTEIN EXPRESSION IN BONE FRACTURE HEALING IN VECTOR AND LMWTg MICE

Trap mRNA of the fracture callus of Vector and LMWTg mice was determined. As shown in Figure 7A compared with PFD3, Trap

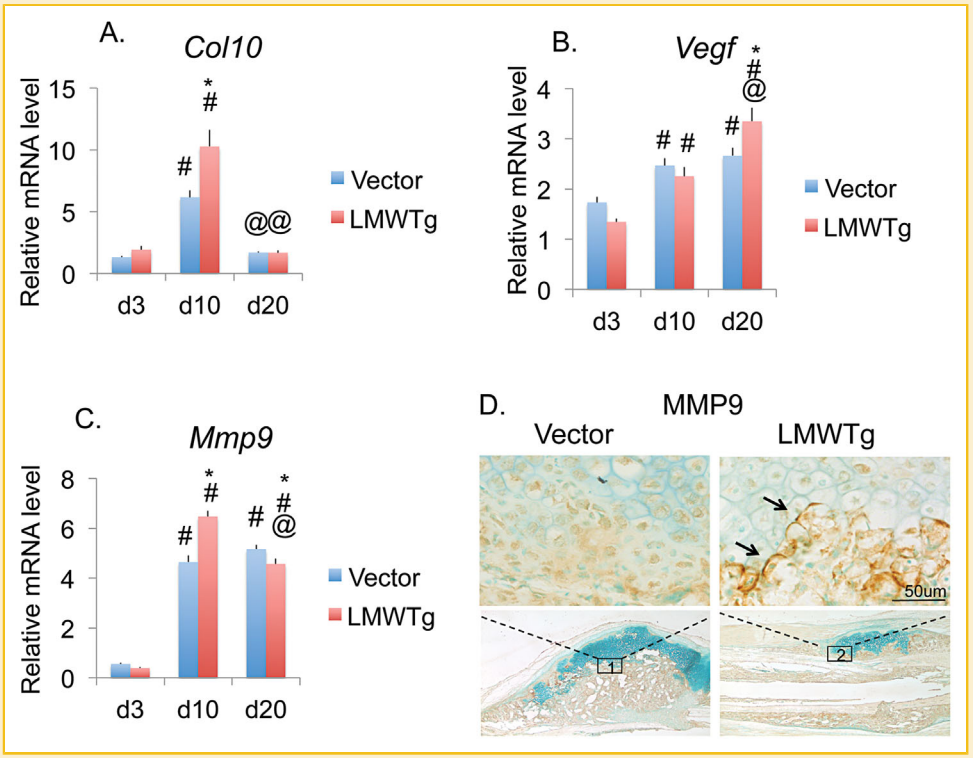

Fig. 6. Col10 mRNA, Vegf mRNA, and Mmp9 mRNA and protein expression in tibial fracture healing in Vector and LMWTg mice. (A) Col10 mRNA in the fracture callus of Vector and LMWTg mice at post fracture day (PFD) 3,10, and 20. Compared to Vector, Col10 mRNA was higher in LMWTg mice at PFD10. Compared to corresponding PFD3, Col10 mRNA was increased in both Vector and LMWTg at PFD10 and returned to PFD3 level at PFD20. n = 7–11. (B) Vegf mRNA expression in the fracture callus of Vector and LMWTg mice at 3,10, and PFD20. Compared to corresponding Vector, Vegf mRNA expression was higher in LMWTg at PFD20. Compared with PFD3, Vegf mRNA was increased at 10 and PFD20 in both Vector and LMWTg mice. There was a further increase at PFD20 in LMWTg compared with PFD10. n = 7–11. (C) Mmp9 mRNA expression in the fracture callus of Vector and LMWTg mice at 3,10, and PFD20. Compared to corresponding Vector, Mmp9 mRNA expression was increased at PFD10 but decreased at PFD20 in MWTg mice. In Vector mice, compared to PFD3, Mmp9 mRNA expression was increased at both 10 and PFD20. In LMWTg mice, Mmp9 mRNA expression was increased at PFD10, then decreased at PFd20. n = 7–11. (D) Immunohistochemistry for MMP9 protein in the fracture callus of Vector and LMWTg mice at PFD10. Note increased MMP9 protein (arrows) in chondrocytes in LMWTg mice. Data are the mean ± SEM. *Compared with corresponding Vector $P < 0.05$; # Compared with corresponding PFD3 $P < 005$; @Compared with corresponding PFD10 $P < 0.05$. For immunohistochemistry staining, all insets are 20× magnification of each figure at 4× magnification.

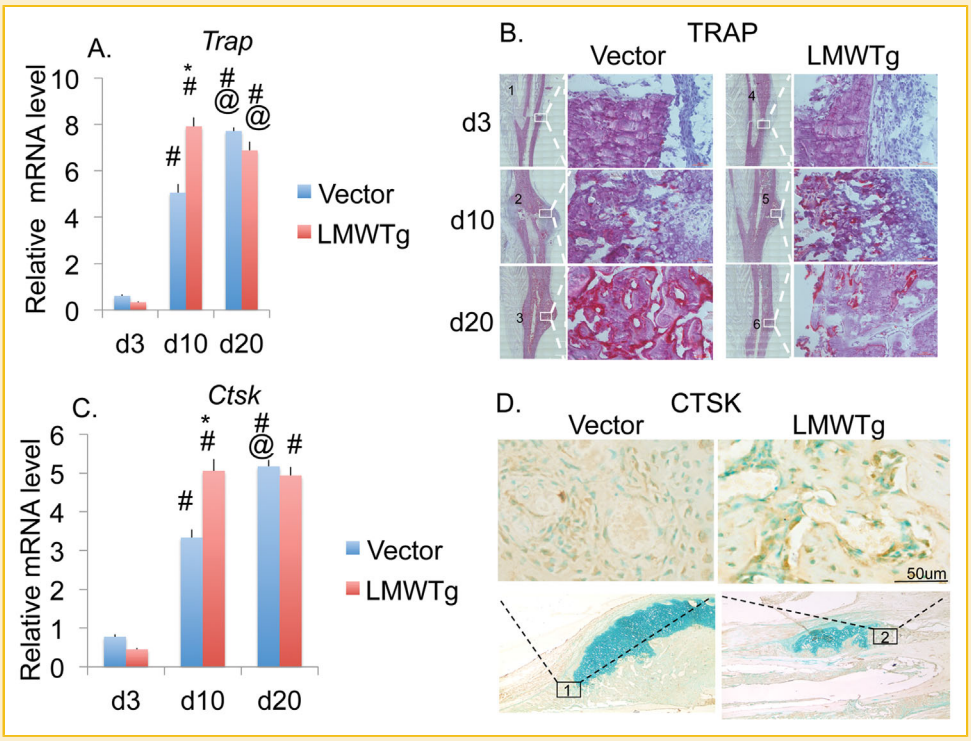

Fig. 7. Trap and Cathepsin K mRNA and protein expression in tibial fracture healing in Vector and LMWTg mice. (A) Trap mRNA in the fracture callus of Vector and LMWTg mice at post fracture day (PFD) 3, 10, and 20. At PFD10, Trap mRNA was increased in LMWTg mice compared with Vector. In Vector mice, Trap mRNA was increased at PFD10, and further increased at PFD20. In LMWTg mice, Trap mRNA was increased at PFD10, then decreased at PFD20. n = 7–11. (B) Histochemistry for TRAP in the fracture callus of Vector and LMWTg mice at 3, 10, and PFD20. In Vector mice, TRAP staining was increased from PFD10 to PFD20. In LMWTg mice, TRAP expression peaked at PFD10. (C) qPCR analysis of Cathepsin K mRNA expression in the fracture callus of Vector and LMWTg mice at 3,10, and PFD20. Compared to Vector, Cathepsin K mRNA expression was higher in LMWTg mice at PFD10. Compared to corresponding PFD3, Cathepsin K mRNA expression is increased in both Vector and LMWTg at 10 and PFD20. There was a further increase at PFD20 compared with PFD10 in Vector mice. n = 7–11. (D) Immunohistochemistry for CATHEPSIN K protein in the fracture callus of Vector and LMWTg mice at PFD10. Note the expression of CATHEPSIN K was higher in LMWTg mice compared with Vector mice. Data are the mean ± SEM. *Compared with corresponding Vector $P < 0.05$; #Compared with corresponding PFD3 $P < 005$; @Compared with corresponding PFD10 $P < 0.05$. For immunohistochemistry staining, all insets are 20× magnification of each figure at 4× magnification.

mRNA was significantly increased at PFD10 and further increased at PFD20 in Vector. In LMWTg mice, Trap mRNA expression peaked at PFD10. At PFD10, Trap mRNA was increased in LMWTg mice compared with corresponding Vector. As shown in Figure 7B, at PFD10 TRAP positive chondroclasts and osteoclasts (OCLs) were found in both cartilage and bony area of callus of Vector and LMWTg, however, there were more TRAP positive OCLs in LMWTg compared with Vector. This difference reflects the fact that the majority of the callus in Vector is still in the chondrogenic phase. Thus there is a delay of bone remodeling in Vector on PFD10. Consistent with this, on PFD20 there were more TRAP positive OCLs in Vector since bone remodeling was almost completed in LMWTg but not in Vector.

Analysis of cathepsin K (Ctsk) mRNA in the fracture callus of Vector and LMWTg mice was determined at 3,10, and PFD20 (Fig. 7C). Compared to Vector, Ctsk mRNA expression was higher in LMWTg mice at PFD10. Compared to corresponding PFD3, Ctsk mRNA expression was increased in both Vector and LMWTg at 10 and PFD20. There was a further increase at PFD20 compared with PFD10 in Vector mice. Cathepsin K protein (CTSK) expression is shown in Figure 7D. On PFD10 CTSK positive chondroclasts that were attached to the cartilage matrix were observed. Immunohistochemistry shows that the predominant localization of CTSK in OCLs and chondroclasts at the osteochondral junction as well as fibroblast like cells. However, there was increased CTSK expression in LMWTg compared with Vector. No CTSK expression was found in the fracture area on PFD3 in either Vector or LMWTg mice and no difference was observed in CTSK expression between Vector and LMWTg on PFD20 (data not shown).

ANALYSIS OF RUNX2, OSTERIX, AND OSTEOCALCIN IN TIBIAL FRACTURE HEALING IN VECTOR AND LMWTg MICE

The time course expression of genes important in osteoblast differentiation was determined in fracture calluses of Vector and LMWTg mice. Runx2 mRNA in the fracture callus of Vector and LMWTg mice is shown in Figure 8A. In both Vector and LMWTg mice, Runx2 mRNA was increased at PFD10 compared with PFD3. At PFD10, Runx2 mRNA was increased in LMWTg compared with corresponding Vector. There was a further increase at PFD20 compared with PFD10 in both Vector and LMWTg. Immunohistochemical labeling for RUNX2

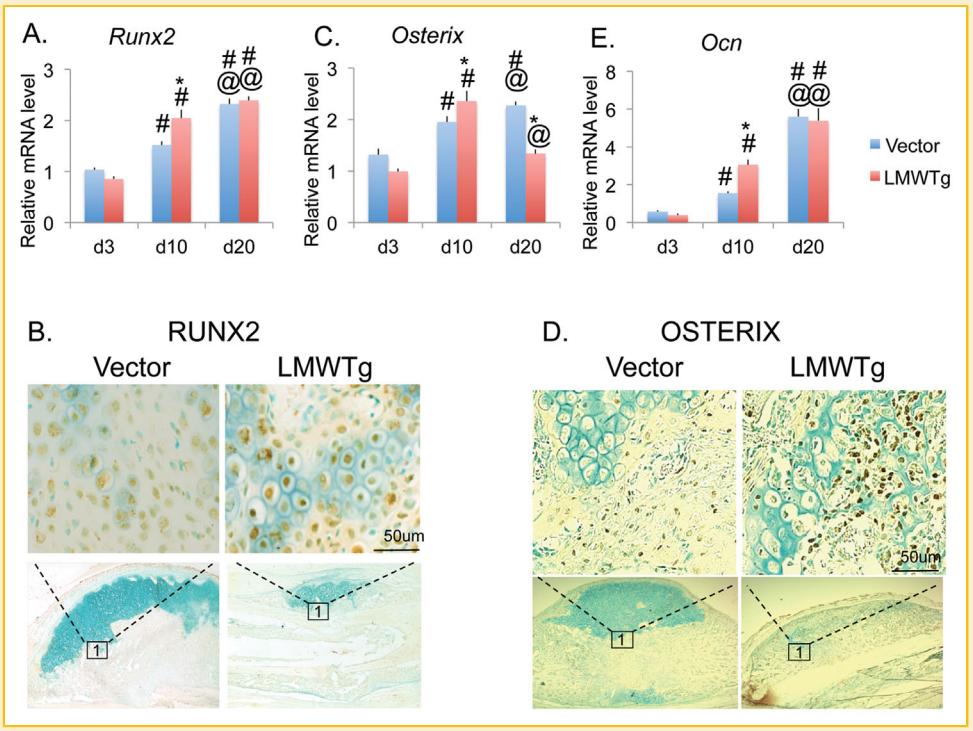

Fig. 8. Runx2, Osterix, and Osteocalcin mRNA and protein expression in tibial fracture healing in Vector and LMWTg mice. (A) Runx2 mRNA in the fracture callus of Vector and LMWTg mice at post fracture day 3, 10, and 20. At PFD10, Runx2 mRNA was increased in LMWTg mice compared with Vector. In both Vector and LMWTg mice, Runx2 mRNA expression was increased at PFD10 compared with PFD3. There was a further increase at 20DPF compared with PFD10 in both Vector and LMWTg. n = 7–11. (B) Immunohistochemistry for RUNX2 protein in the fracture callus of Vector and LMWTg mice at PFD10. Note the increased expression of RUNX2 in LMWTg mice. (C) qPCR analysis of Osterix mRNA expression in the fracture callus of Vector and LMWTg mice at 3,10, and PFD20. Compared to Vector, Osterix mRNA expression was higher at PFD10, but lower at PDFD20 in LMWTg mice. In Vector mice, Osterix mRNA expression was increased at PFD10 compared with PFD3, and there was a further increase at PFD20. In LMWTg mice Osterix mRNA increased at PFD10 compared with PFD3 and was decreased at PFD20. n = 6–11. (D) Immunohistochemistry for OSTERIX protein in the fracture callus of Vector and LMWTg mice at PFD10. Note increased OSTERIX in LMWTg mice. (E) Ocn mRNA in the fracture callus of Vector and LMWTg mice at 3, 10, and PFD20. At PFD10, Ocn mRNA was higher in LMWTg mice compared with Vector. In both Vector and LMWTg mice, Ocn mRNA expression was increased at PFD10 compared with PFD3 and further increased at 20DPF. n = 7–11. Data are the mean ± SEM. *Compared with corresponding Vector $P < 0.05$; #Compared with corresponding PFD3 $P < 005$; @Compared with corresponding PFD10 $P < 0.05$. For immunohistochemistry staining, all insets are 20× magnification of each figure at 4× magnification.

protein was also determined. On PFD10 (Fig. 8B) RUNX2 protein was expressed in the area of membranous and endochondral ossification sites (inset1), in the periosteal cells close to the fracture site, chondrocytes, osteoblast, and osteocyte surrounding woven bone, as well as fibroblast like cells. The overall expression level of RUNX2 protein was increased in LMWTg mice compared with Vector.

Analysis of Osterix mRNA in the fracture callus of Vector and LMWTg mice is shown in Figure 8C. Compared to Vector, Osterix mRNA is significantly higher at PFD10, but lower at PFD20 in LMWTg mice. In Vector mice, Osterix mRNA was increased at PFD10 compared with PFD3 and there was a further increase at PFD20. Osterix protein was detected in the fracture callus in osteoblasts and osteocytes in newly formed bone (Fig. 8D), but staining was stronger in LMWTg. The strongest labeling in LMWTg was observed in the periosteum over the callus and junction of bony and cartilage area (inset 1). In addition, there was a lack of staining in the hypertrophic chondrocytes of both Vector and LMWTg mice. On PFD3, there was increased osterix expression in the periosteum adjacent to the fracture site in LMWTg compared with Vector (data not shown). On PFD20, osterix expression remained higher in osteoblast and osteocytes of LMWTg compared with Vector (data not shown). Osteocalcin (Ocn) is a terminal osteoblast differentiation marker gene. As shown in Figure 8E at PFD10, Ocn mRNA was higher in LMWTg mice compared with Vector. In both Vector and LMWTg mice, Ocn mRNA expression was increased at PFD10 compared with PFD3 and further increased at PFD20.

DISCUSSION

FGF2 is an important growth factor in bone formation and remodeling [Hurley et al., 2008] and as shown from disruption of the Fgf2 gene, is also important in maintaining bone mass at least in mice [Montero et al., 2000]. FGF2 is among the growth factors/cytokines that are present in skeletal tissue, expressed in fracture callus, and involved in the repair process in response to trauma [Schmid et al., 2009]. We hypothesized that targeted expression of FGF2 in osteoblast lineage cells would set the healing cascade into motion at a faster pace, resulting in a more rapid progression through the stages of repair, and therefore accelerate the healing process. The current study shows that

overexpression of LMWFGF2 accelerated the healing process by enhancing the differentiation of chondrocyte and osteoblast precursors. This accelerated fracture repair in LMWTg mice was associated with differential FGFR expression. Interestingly, compared with Vector, enhanced early expression of FGFR3 was observed at PFD3 in LMWTg. Studies by Rundle et al. [2002]; showed increased FGFR3 expression in mesenchymal cells, prehypertrophic and hypertrophic chondrocytes of the fracture callus at PFD10 during fracture healing. Nakajima et al. [2003] reported that prehypertrophic chondrocytes strongly expressed FGFR3 and proposed that FGFR3 may promote fracturing healing by accelerating the replacement of the cartilaginous callus with bone and would be consistent with accelerated fracture repair observed in LMWTg mice.

Normal fracture healing and bone repair is a complex process involving multiple stages. Studies have shown that immediately following injury, local hemorrhage results in hematoma, which within 24 h is replaced by a poorly organized cellular matrix, which raises the periosteum away from the bone cortex to form the osteoblast collar [MacMahon and Eustace, 2006]. Our observation of increased FGF2 labeling in the periosteal layer adjacent to the fracture site of LMWTg at PFD3 would support increased periosteal cell proliferation and differentiation that could contribute to accelerated fracture healing in these mice.

Accelerated fracture healing in LMWTg mice provided an opportunity to determine whether FGF2 enhanced fracture healing by modulating the temporal or level of expression of known and novel genes during repair. One of the earliest genes for chondrogenesis expressed during repair is the transcription factor Sox9. We observed a differential temporal expression in Vector versus LMWTg wherein Sox9 was significantly increased at PFD3 in LMWTg when there was no evidence of a fracture callus in either genotype. These results are consistent with increased Sox9 expression in early osteochondro-progenitors facilitated by enhanced FGF2 expression.

The present study also demonstrated that the fracture callus was significantly smaller in LMWTg fractured tibiae and that bridging of the tibial fragments and healing occurred at an earlier time point compared with Vector control mice. Both of these observations are in contrast to the study of [Nakajima et al., 2001], who reported that a single percutaneous injection of FGF2 into the fracture site of a closed rat tibial fracture immediately after fracture resulted in larger callus at each stage of fracture healing but not to rapid healing. Although the time points examined in the present study (PFD3, PFD10, and PFD20) differed from the time points (PFD7, PFD14, PFD21, and PFD28) examined by Nakajima et al. [2001], we did not observe a larger callus at any time point. Other differences between the fracture models included the gender and species (male rats vs. female mice). Another difference is the fact that in the studies of Nakajima et al. [2001], FGF2 was administered as a single injection immediately after fracture. Consistent with our observation of accelerated fracture healing, a previous study [Baron et al., 1994], found that continuous in vivo infusion of FGF2 into the rabbit proximal tibial growth plate accelerated ossification and differentiation of chondrocytes. These authors postulated that FGF2 induced vascular invasion could have contributed to the accelerated ossification of the growth plate cartilage. Although we examined vascular invasion by CD-31-capillary staining at each time point, we did not consistently observe increased vascularity in the LMWTg fracture calluses. However, we did observe a greater increase in angiogenic factors including several PDGF genes [Andrew et al., 1995] as well as VEGF [Lienau et al., 2009] protein in LMWTg compared with Vector.

It is also possible that the effects of LMW are indirect since FGF2 regulates the production of other growth factors such as BMP2 [Balint et al., 2003], which is a potent inducer of fracture healing [Tsuji et al., 2006]. Although we observed increased BMP2 expression in the healing fracture over the 20 day period, the mRNA and protein levels were similar in both genotypes (data not shown). Thus increased BMP2 is not the mediator of accelerated fracture healing in the LMWTg mice.

PDGF genes are important in regulating mesenchymal cell differentiation and have potent effects on chondrocytes and osteoblasts [Andrew et al., 1995], however, there are no data showing that during fracture repair LMW regulates PDGF gene expression. PDGF-A and B are expressed during normal fracture healing and while PDGF-A was widely expressed by many cell types PDGF-B appeared to be expressed primarily in osteoblasts during the stage of bone formation during fracture healing [Andrew et al., 1995]. Interestingly in the present study, the temporal and level of Pdgfa mRNA was similar in both genotypes and while the temporal pattern of expression of Pdgfb mRNA was similar in both genotypes, there was enhanced expression in LMWTg at PFD10 consistent with increased bone formation. Although the temporal pattern of Pdgfc and Pdgfd were similar in Vector and LMWTg, Pdgfc and Pdgfd mRNA were significantly increased at PFD10 in LMWTg. PDGF-C and PDGF-D have been implicated in angiogenesis, embryogenesis, and platelet activation and LMW was reported to increase Pdgfc in smooth muscle cells [Midgley and Khachigian, 2004]. However, this is the first report that Pdgfc and Pdgfd are expressed during fracture repair and that LMW regulates their expression during fracture repair. The significance of LMW regulation of Pdgfc and Pdgfd during fracture healing is unclear and requires further investigation.

Previous studies have shown that MMP9, MMP13, and CTSK were up-regulated during the first and second week of fracture healing [Uusitalo et al., 2000]. However, there are no data on FGF2 regulation of these proteolytic enzymes during fracture repair. The current study shows that overexpression of LMW in osteoblasts caused a greater increase in MMP9 and CTSK that are important in remodeling of the extracellular matrix. Furthermore the temporal pattern of TRAP positive osteoclasts in LMWTg is consistent with accelerated remodeling of the new bone.

We also examined the expression of RUNX2 since previous studies have shown that RUNX2 expression is increased during fracture healing [Kawahata et al., 2003]. Therefore our observation of increased RUNX2 protein in LMWTg mice is consistent with previous reports.

Studies have also suggested an important role for the zinc finger protein osterix in mediating endochondral ossification during fracture repair [Kaback et al., 2008], however, there are no studies on FGF2 regulation of osterix during fracture healing. Thus, the present study is the first report that LMW FGF2 increases osterix during fracture healing.

Osteocalcin is a terminal osteoblastic differentiation marker gene. It plays important roles in the early stage of bone healing and regulation of osteoblastic activity [Hauschka and Wians, 1989]. During the early bone healing stage, osteocalcin is chemotactic for the osteoclastic cells [Glowacki and Lian, 1987]. In the current study, osteocalcin gene expression was found to be higher in LMWTg mice. This increase was correlated with histology observation of increased bony/total callus area in LMWTg mice.

In conclusion, the current study provides in vivo evidence for an important role for the LMW FGF2 in bone fracture healing. Accelerated bone formation was due to faster progression through the stages of cartilage formation, bone union, and callus remodeling. Overexpression of FGF2 resulted in increased numbers of osteoblasts around the fracture area that accelerated intra-membranous bone formation. Since accelerated fracture healing in LMWTg mice was associated with a temporal change or increased Sox9, VEGF, PDGFs, RUNX2, and osterix expression, we postulate that over expression of LMW accelerated the fracture healing process due to its effects on factors that are important in chondro-osteo progenitor differentiation.

ACKNOWLEDGMENTS

This work was supported in part by the National Institute of Aging under award number R01AG021189. The content is solely the responsibility of the authors and does not necessarily represent the official views of the National Institutes of Health.

REFERENCES

Amizuka N,Davidson D, Liu HL, Valverde-Franco G, Chai S, Maeda T, Ozawa H, Hammond V, Ornitz DM, Goltzman D, Henderson JE. 2004. Signalling by fibroblast growth factor receptor 3 and parathyroid hormone-related peptide coordinate cartilage and bone development. Bone 34:13–25.

Andrew JG, Hoyland JA, Freemont AJ, Marsh DR. 1995. Platelet-derived growth factor expression in normally healing human fractures. Bone 16:455–460.

Balint E, Lapointe D, Drissi H, van der Meijden C, Young DW, van Wijnen AJ, Stein JL, Stein GS, Lian JB. 2003. Phenotype discovery by gene expression profiling: Mapping of biological processes linked to BMP-2-mediated osteoblast differentiation (vol 89, pg 401, 2003). J Cell Biochem 89:862–862.

Baron J, Klein KO, Yanovski JA, Novosad JA, Bacher JD, Bolander ME, Cutler GB. 1994. Induction of growth-plate cartilage ossification by basic fibroblast growth-factor. Endocrinology 135:2790–2793.

Bland YS, Critchlow MA, Ashhurst DE. 1995. Exogenous fibroblast growth factors-1 and -2 do not accelerate fracture healing in the rabbit. Acta orthopaedica Scandinavica 66:543–548.

Bonnarens F, Einhorn TA. 1984. Production of a standard closed fracture in laboratory animal bone. J Orthop Res 2:97–101.

Bostrom MP, Lane JM, Berberian WS, Missri AA, Tomin E, Weiland A, Doty SB, Glaser D, Rosen VM. 1995. Immunolocalization and expression of bone morphogenetic proteins 2 and 4 in fracture healing. J Orthop Res 13:357–367.

Einhorn TA. 1998. The cell and molecular biology of fracture healing. Clin Orthop Relat Res 355 Suppl:S7–21.

Fei Y, Gronowicz G, Hurley MM. 2013. Fibroblast growth factor-2, bone homeostasis and fracture repair. Curr Pharm Des 19:3354–3363.

Florkiewicz RZ, Sommer A. 1989. Human basic fibroblast growth factor gene encodes four polypeptides: Three initiate translation from non-AUG codons. Proc Natl Acad Sci USA 86:3978–3981.

Glowacki J, Lian JB. 1987. Impaired recruitment and differentiation of osteoclast progenitors by osteocalcin-deplete bone implants. Cell Differ 21:247–254.

Gospodarowicz D. 1990. Fibroblast growth factor. Chemical structure and biologic function. Clin Orthop Relat Res 257:231–248.

Hadjiargyrou M, O'Keefe RJ. 2014. The convergence of fracture repair and stem cells: Interplay of genes, aging, environmental factors and disease. J Bone Miner Res 29:2307–2322.

Hauschka PV, Wians FH, Jr. 1989. Osteocalcin-hydroxyapatite interaction in the extracellular organic matrix of bone. Anat Rec 224:180–188.

Hiltunen A, Vuorio E, Aro HT. 1993. A standardized experimental fracture in the mouse tibia. J Orthop Res 11:305–312.

Hurley MM, Naski M, Marie PJ. 2008. Fibroblast growth factor and fibroblast growth factor receptor families in bone. In: J. Bilezikian LGRaTM, editors. Principles of bone biology. Academic Press pp 1103–1132.

Kaback LA, Soung do Y, Naik A, Smith N, Schwarz EM, O'Keefe RJ, Drissi H. 2008. Osterix/Sp7 regulates mesenchymal stem cell mediated endochondral ossification. J Cell Physiol 214:173–182.

Kalajzic I, Kalajzic Z, Kaliterna M, Gronowicz G, Clark SH, Lichtler AC, Rowe D. 2002. Use of type I collagen green fluorescent protein transgenes to identify subpopulations of cells at different stages of the osteoblast lineage. J Bone Miner Res 17:15–25.

Kawaguchi H, Kurokawa T, Hanada K, Hiyama Y, Tamura M, Ogata E, Matsumoto T. 1994. Stimulation of fracture repair by recombinant human basic fibroblast growth factor in normal and streptozotocin-diabetic rats. Endocrinology 135:774–781.

Kawaguchi H, Nakamura K, Tabata Y, Ikada Y, Aoyama I, Anzai J, Nakamura T, Hiyama Y, Tamura M. 2001. Acceleration of fracture healing in nonhuman primates by fibroblast growth factor-2. J Clin Endocrinol Metab 86:875–880.

Kawaguchi H, Oka H, Jingushi S, Izumi T, Fukunaga M, Sato K, Matsushita T, Nakamura K. 2010. A local application of recombinant human fibroblast growth factor 2 for tibial shaft fractures: A randomized, placebo-controlled trial. J Bone Miner Res 25:2735–2743.

Kawahata H, Kikkawa T, Higashibata Y, Sakuma T, Huening M, Sato M, Sugimoto M, Kuriyama K, Terai K, Kitamura Y, Nomura S. 2003. Enhanced expression of Runx2/PEBP2alphaA/CBFA1/AML3 during fracture healing. J Orthop Sci 8:102–108.

Komaki H, Tanaka T, Chazono M, Kikuchi T. 2006. Repair of segmental bone defects in rabbit tibiae using a complex of beta-tricalcium phosphate, type I collagen, and fibroblast growth factor-2. Biomaterials 27:5118–5126.

Li MQ, Amizuka N, Takeuchi K, Freitas PHL, Kawano Y, Hoshino M, Oda K, Nozawa-Inoue K, Maeda T. 2006. Histochemical evidence of osteoclastic degradation of extracellular matrix in osteolytic metastasis originating from human lung small carcinoma (SBC-5) cells. Microsc Res Tech 69:73–83.

Lienau J, Schmidt-Bleek K, Peters A, Haschke F, Duda GN, Perka C, Bail HJ, Schutze N, Jakob F, Schell H. 2009. Differential regulation of blood vessel formation between standard and delayed bone healing. J Orthop Res 27:1133–1140.

MacMahon P, Eustace SJ. 2006. General principles. Semin Musculoskelet Radiol 10:243–248.

Midgley VC, Khachigian LM. 2004. Fibroblast growth factor-2 induction of platelet-derived growth factor-C chain transcription in vascular smooth muscle cells is ERK-dependent but not JNK-dependent and mediated by Egr-1. J Biol Chem 279:40289–40295.

Montero A, Okada Y, Tomita M, Ito M, Tsurukami H, Nakamura T, Doetschman T, Coffin JD, Hurley MM. 2000. Disruption of the fibroblast growth factor-2 gene results in decreased bone mass and bone formation. J Clin Invest 105:1085–1093.

Nakajima F, Ogasawara A, Goto K, Moriya H, Ninomiya Y, Einhorn TA, Yamazaki M. 2001. Spatial and temporal gene expression in chondrogenesis during fracture healing and the effects of basic fibroblast growth factor. J Orthop Res 19:935–944.

Nakamura T, Hara Y, Tagawa M, Tamura M, Yuge T, Fukuda H, Nigi H. 1998. Recombinant human basic fibroblast growth factor accelerates fracture healing by enhancing callus remodeling in experimental dog tibial fracture. J Bone Miner Res 13:942–949.

Pfaffl MW. 2001. A new mathematical model for relative quantification in real-time RT-PCR. Nucleic Acids Res 29:e45.

Radomsky ML, Aufdemorte TB, Swain LD, Fox WC, Spiro RC, Poser JW. 1999. Novel formulation of fibroblast growth factor-2 in a hyaluronan gel accelerates fracture healing in nonhuman primates. J Orthop Res 17:607–614.

Radomsky ML, Thompson AY, Spiro RC, Poser JW. 1998. Potential role of fibroblast growth factor in enhancement of fracture healing. Clin Orthop Relat Res S283–S293.

Schmid GJ, Kobayashi C, Sandell LJ, Ornitz DM. 2009. Fibroblast growth factor expression during skeletal fracture healing in mice. Dev Dyn 238:766–774.

Scully SP, Joyce ME, Abidi N, Bolander ME. 1990. The use of polymerase chain-reaction generated nucleotide-sequences as probes for hybridization. Mol Cell Probes 4:485–495.

Tanaka T, Kitasato S, Chazono M, Kumagae Y, Iida T, Mitsuhashi M, Kakuta A, Marumo K. 2012. Use of an injectable complex of beta-tricalcium phosphate granules, hyaluronate, and fibroblast growth factor-2 on repair of unstable intertrochanteric fractures. Open Biomed Eng J 6:98–103.

Tokuda H, Takai S, Hanai Y, Harada A, Matsushima-Nishiwaki R, Kato H, Ogura S, Kozawa O. 2008. Potentiation by platelet-derived growth factor-BB of FGF-2-stimulated VEGF release in osteoblasts. J Bone Miner Metab 26:335–341.

Tsuji K, Bandyopadhyay A, Harfe BD, Cox K, Kakar S, Gerstenfeld L, Einhorn T, Tabin CJ, Rosen V. 2006. BMP2 activity, although dispensable for bone formation, is required for the initiation of fracture healing. Nat Genet 38:1424–1429.

Uusitalo H, Hiltunen A, Soderstrom M, Aro HT, Vuorio E. 2000. Expression of cathepsins B, H, K, L, and and matrix metalloproteinases 9 and 13 during chondrocyte hypertrophy and endochondral ossification in mouse fracture callus. Calcif Tissue Int 67:382–390.

Xiao L, Liu P, Sobue T, Lichtler A, Coffin JD, Hurley MM. 2003. Effect of overexpressing fibroblast growth factor 2 protein isoforms in osteoblastic ROS 17/2.8 cells. J Cell Biochem 89:1291–1301.

Xiao L, Ueno D, Catros S, Homer-Bouthiette C, Charles L, Kuhn L, Hurley MM. 2014. Fibroblast growth factor-2 isoform (low molecular weight/18kDa) overexpression in preosteoblast cells promotes bone regeneration in critical size calvarial defects in male mice. Endocrinology 155:965–974.

Xiao LP, Liu P, Li XF, Doetschman T, Coffin JD, Drissi H, Hurley MM. 2009. Exported 18-kDa isoform of fibroblast growth factor-2 is a critical determinant of bone mass in mice. J Biol Chem 284:3170–3182.

Yamagiwa H, Tokunaga K, Hayami T, Hatano H, Uchida M, Endo N, Takahashi HE. 1999. Expression of metalloproteinase-13 (collagenase-3) is induced during fracture healing in mice. Bone 25:197–203.

SUPPORTING INFORMATION

Additional supporting information may be found in the online version of this article at the publisher's web-site.